IEEE Access
Multidisciplinary ⋮ Rapid Review ⋮ Open Access Journal

Received 4 July 2022, accepted 19 July 2022, date of publication 26 July 2022, date of current version 29 July 2022.

Digital Object Identifier 10.1109/ACCESS.2022.3193692

RESEARCH ARTICLE

A Wideband Scanning Circularly Polarized Array Antenna Based on the Shorted Transmission Line Model

MING-YANG ZHAO[1,2], YI-JUN ZHU[1], (Member, IEEE), TAO WANG[1], TIAN-PENG LI[1], BEN-LONG XIAO[2], FENG-LIANG NIU[2], AND XUE LEI[1]

[1]School of Information Engineering University, Zhengzhou 450001, China
[2]State Key Laboratory of Complex Electromagnetic Environment Effects on Electronics and Information System, Luoyang 471003, China

Corresponding author: Ming-Yang Zhao (lingyang20070603@163.com)

This work was supported in part by the National Natural Science Foundation of China (NSFC) under Grant 61671477 and Grant 61901524, and in part by the China Postdoctoral Science Foundation under Grant 2019M663477.

ABSTRACT Due to the huge potential of application in the communications, electronic jamming, and radar fields, circularly polarized (CP) array antennas with wide axial ratio (AR) scanning performance at wide frequency bandwidth have received great attention. A wideband scanning CP planar array antenna built by new, tightly coupled dipole array (CP-TCDA) elements, which have achieved promising results in terms of both scanning AR bandwidth and angle range in all scanning planes, is presented in this paper. Based on the shorted transmission line model, a CP-TCDA element arranged along the $\pm 45°$ direction is constructed, which can shift the middle-frequency scanning blind zone out of band and thus obtain a wideband scanning AR bandwidth. Furthermore, the proposed CP-TCDA element adopts four shorting pins and four square parasitic strips, which improve wide-angle CP performance for *xz*-plane and diagonal-plane scans, respectively. An 8×8 left-handed CP planar array antenna based on the proposed CP-TCDA elements is designed and prototyped. The results show that the array antenna is able to operate over a 3:1 (4–12 GHz) overlapping bandwidth, and it meets the requirements of AR < 3 dB and active VSWR < 2.9 within a $\pm 45°$ scanning angle range.

INDEX TERMS Array antenna, circularly polarized, phased antenna, scanning antennas.

I. INTRODUCTION

Beam scanning antennas are a typical type of array antennas and the beam control is realized by changing the excitation phase of the antenna elements. Beam scanning antennas have been widely used in military and civilian fields because of the flexibility and agility of beam pointing, and the ability of searching and tracking target signals on moving carriers [1]. Particularly, with the increasing number of modern electronic devices and large buildings, our electromagnetic environment becomes more complex. Compared with linearly polarized antennas, circularly polarized (CP) antennas have many unique advantages, such as being insensitive to electromagnetic wave polarization, suppressing multipath interference, and avoiding Faraday rotation effects [2], [3]. CP antennas can better ensure the quality of signal transmission than linearly polarized antennas, so CP beam-scanning antennas are widely used in wireless communication, satellite communication, remote sensing detection, electronic jamming, radar, navigation, and other fields. Usually, the axial ratio (AR) of the main beam will deteriorate when the scanning angle is moved away from broadside, so the CP array antenna with wide AR scanning performance at wide frequency bandwidth, hereinafter referred to as wideband scanning CP array antenna, is hard to obtain.

Existing CP beam scanning antennas mainly include sequential rotation CP spiral antenna [4], dielectric resonator antenna [5], switched-beam array antenna with Butler matrix [6], space-fed multi-beam reflectarray [7],

The associate editor coordinating the review of this manuscript and approving it for publication was Giorgio Montisci.

TABLE 1. Performance comparison of CP beam scanning antennas and CP TCDA antennas.

Ref.	Number of elements	Size (λ_{low}^3)	Scanning angle range	Relative bandwidth	Peak gain (dBic)	Antenna efficiency
[2]	4×16	**	±40°	2%	**	**
[3]	16×16	##$9.06\lambda_{low}\times9.06\lambda_{low}\times0.48\lambda_{low}$	±40°	10%	28.3	**
[4]	4×4	$2.58\lambda_{low}\times2.48\lambda_{low}\times0.216\lambda_{low}$	±25°	40%	**	**
[5]	2×2	$1.5\lambda_{low}\times1.5\lambda_{low}\times0.17\lambda_{low}$	±22°	3.8%	6.6	**
[6]	6×6	**	±60°	2%	17.5	**
[7]	**	$12.27\lambda_{low}\times12.27\lambda_{low}\times5.45\lambda_{low}$	±29°	13.6%	24.6	> 15%
[8]	1×8	**	±49°	3%	13.4	## > 52%
[9]	1×10	**	−13°–28°	40%	12.72	## > 32%
[10]	1×8	**	±57°	##20%	**	**
[18]	4×4	$1.25\lambda_{low}\times1.25\lambda_{low}\times0.09\lambda_{low}$	Fixed-beam	82%	**	**
[19]	8×8	$2.89\lambda_{low}\times2.89\lambda_{low}\times0.28\lambda_{low}$	Fixed-beam	44.9%	20.9	> 34%
[20]	Single antenna	$0.67\lambda_{low}\times0.67\lambda_{low}\times0.16\lambda_{low}$	Fixed-beam	94.2%	7.04	> 70%
[21]	Single antenna	$0.8\lambda_{low}\times0.8\lambda_{low}\times0.15\lambda_{low}$ (circular aperture)	Fixed-beam	77%	**	**
[22]	16*16 (simulation)	$3.52\lambda_{low}\times3.52\lambda_{low}\times0.067\lambda_{low}$	±60°(AR < 4 dB)	15%	**	**
This work	8×8	$\mathbf{1.33\lambda_{low}\times1.33\lambda_{low}\times0.11\lambda_{low}}$	**±45°**	**100%**	**22.37**	**> 70%**

** Authors did not supply the values.
Authors did not supply the exact values, and the data are obtained by extrapolating from the given information.
λ_{low} represents the free-space wavelength at the lowest operating frequency.

reconfigurable patch array antenna [8], frequency scanning leaky wave antenna [9], and amplitude- and phase-controlled dual-polarized antennas [10]. The above CP beam scanning antennas have achieved promising results in some respects, yet leave a lot to be desired in terms of wideband scanning, particularly in the scanning AR bandwidth and angle range in all scanning planes.

In recent years, the tightly coupled dipole array (TCDA) antenna has gained wide attention because it expands the scanning bandwidth due to the coupling of its elements [11]. In order to improve the scanning bandwidth of TCDA antennas, one important aspect is to suppress the in-band common mode resonance; for example, by using a TCDA antenna with integrated balun [12], or planar ultrawideband modular antennas based on shorted via [13] or capacitively loaded via [14]. However, most reported TCDA antennas worked with linear polarization or dual linear polarization (DP) [12]–[17], and few papers deal with CP-TCDA antenna. A 4 × 4 CP tightly coupled crossed dipole array antenna was designed in [18]. However, due to the use of absorbers, the real gain of the antenna was about 4 dB lower than the ideal gain. Bold-C spiral array elements were used to design an 8 × 8 CP array antenna in [19], but the AR bandwidth was dependent on the oversampling spacing. It is worth noting that these CP-TCDA antennas only achieved wideband CP, without considering scanning [18]–[21]. Recently, Son *et al.* [22] reported a CP tightly-coupled array with chamfered corners and etched cross slot patch elements. However, the simulated 3dB AR bandwidth is only 15%.

In this paper, based on the wideband CP characteristics of double-feed structures [23] and the wide-angle scanning characteristics of TCDA antennas, we construct a low-profile CP-TCDA element arranged along the ±45° direction. An 8 × 8 left-handed CP (LHCP) planar array antenna based on the proposed CP-TCDA elements is fabricated and measured. The measured results show that the antenna has a 3:1 (4–12 GHz) overlapping bandwidth (the overlapping AR < 3 dB and active VSWR < 2.9 bandwidths), i.e., 100% relative bandwidth, within a ±45° scanning range. Our planar array antenna has great application potential in vehicle, airborne, space-borne, and missile-borne radio frequency front-ends. To the best of our knowledge, there has been no report where the CP beam scanning antenna has achieved a 100% relative bandwidth within a ±45° scanning range. Table 1 shows the comparison between several typical CP beam scanning antennas and the fixed beam CP TCDA antennas. It can be seen that the proposed planar array antenna based on the proposed CP-TCDA elements has achieved good AR bandwidth and scanning angle performance. The novel features of the antenna are as follows.

(1) We have established an analytic model of the in-band scanning blind zone. Although the introduction of the tight coupled environment mitigates the low-frequency AR bandwidth limit, it also results in the appearance of a scanning blind zone. By equating Reference Element I arranged along the grid direction (Figure 1), which is nonradiating, with a $\lambda_g/4$ shorted two-wire transmission line, where λ_g is the waveguide wavelength, we establish a relationship between the element structure parameters and the frequency corresponding to the scanning blind zone. The theoretical results are in good agreement with the simulation results, with only a 5.3% frequency error.

(2) We have also verified the solution for the in-band scanning blind zone. Based on the short-circuited transmission line model, we constructed a CP-TCDA element arranged along the ±45° direction (Figure 6), which can shift the middle-frequency scanning blind zone out of band, so as to achieve a wide scanning AR band.

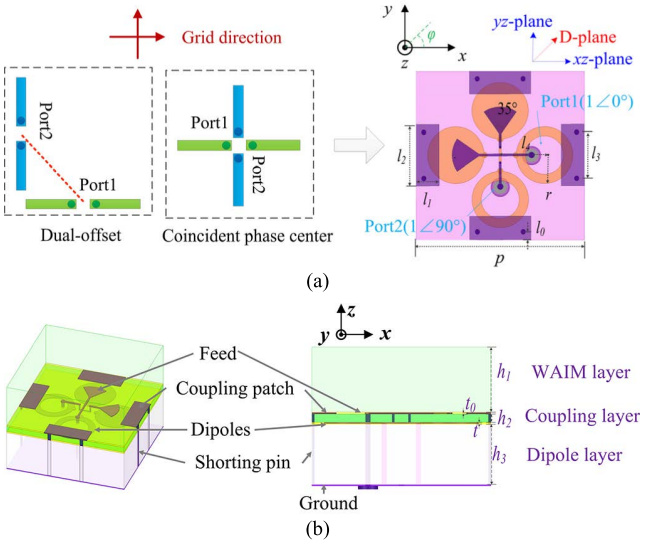

FIGURE 1. Reference element I arranged along the grid direction. (a) Top view. (b) Perspective view.

(3) A comprehensive scheme to improve the scanning angle range is studied. Four shorting pins were introduced to solve the problem of AR degradation in the *xz*-plane caused by common-mode resonance, and four square parasitic strips were added to improve the CP performance of the diagonal-plane (D-plane) scans. The combination of the two methods achieves a wide-angle scanning CP in all scanning planes.

II. THEORETICAL MODEL

It is a challenge for the CP beam scanning array antenna to achieve a 3:1 bandwidth within a ±45° scanning range. Before the introduction of the proposed CP-TCDA element (Figure 6), we first discuss the problems faced by Reference Element I, and we then propose a simple theoretical model of a shorted two-wire transmission line. Based on the theoretical model, we explain the principle of Reference Element II (Figure 5) shifting the scanning blind zone to the low frequency band.

A. CP-TCDA ELEMENT ARRANGED ALONG THE GRID DIRECTION

The DP TCDA antenna achieved promising results in terms of scanning bandwidth and scanning angle. However, the traditional DP TCDA antenna usually adopts a dual-offset topology with a grid layout, as shown in Figure 1(a). The dual-offset topology can reduce the undesired coupling between orthogonal array elements [24], yet this topology is a disaster for CP beam scanning array antennas, because the AR performance deteriorates at wide steering angles and the high frequency band [25]. Therefore, in order to implement wideband scanning for the CP array antenna, the phase centers of the orthogonal dipoles should coincide.

Figure 1 shows the coincident phase center CP element designed based on the concept of the DP TCDA antenna, with a grid layout, and it is referred to as Reference Element I.

TABLE 2. Parameters of reference element I.

Parameter	Value (mm)	Parameter	Value (mm)	Parameter	Value (mm)
l_0	0	l_4	3.4	p	12
l_1	1.5	h_1	3.7	r	1.85
l_2	4	h_2	0.254	t	0.1
l_3	3	h_3	3.7	t_0	0.018

Reference Element I has three layers; these are, from bottom to top, the dipole layer, the coupling layer, and the wide angle impedance matching (WAIM) layer. F_4B ($\varepsilon_r = 2.2$ and $\tan\delta = 0.001$) is used as the dielectric substrate for all three layers, and the thickness t_0 of copper foil of each layer is 0.018 mm. A prepreg of Rogers 4450F is used for layer bonding. The relative dielectric constant and loss tangent of the prepreg are 3.52 and 0.004, respectively, and the thickness is 0.1 mm. In order to avoid the intersection of the coupled feeding structure, an overpass structure is used in the design to lead the signal to the upper surface of the dipole layer, and then two shorting pins are used to lead it back to the coupling layer. The main parameters of Reference Element I are shown in Table 2.

For ease of analysis, the $\varphi = 0°$ plane is defined as the *xz*-plane, the $\varphi = 90°$ plane as the *yz*-plane, and the $\varphi = 45°$ plane as the D-plane, as shown in Figure 1(a). Element simulation is carried out under two-dimensional periodic boundary conditions. Figure 2 shows the AR curve of Reference Element I during broadside and *xz*-plane/D-plane scanning. When the antenna is scanned, unbalanced push-pull current and common mode resonance may appear, resulting in deterioration of low-frequency AR [15]. It can be seen that the introduction of the tightly coupled environment (that is, the grounded coupling patch) mitigates the low-frequency AR bandwidth limitation.

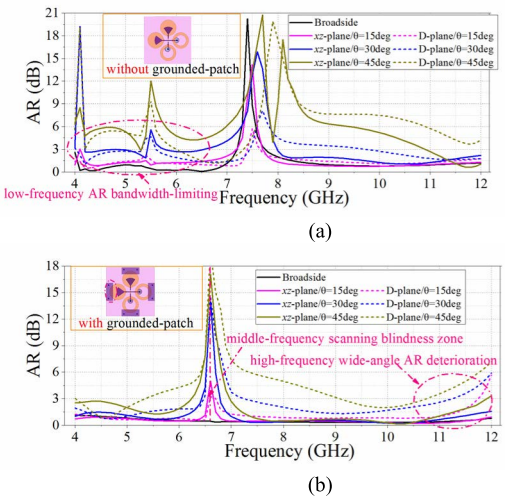

FIGURE 2. AR curves. (a) Without grounded patch. (b) Reference element I.

We aim to achieve the design objective of wideband scanning CP, that is, a 3:1 overlapping bandwidth within a ±45° scanning range. Reference Element I has a limited AR

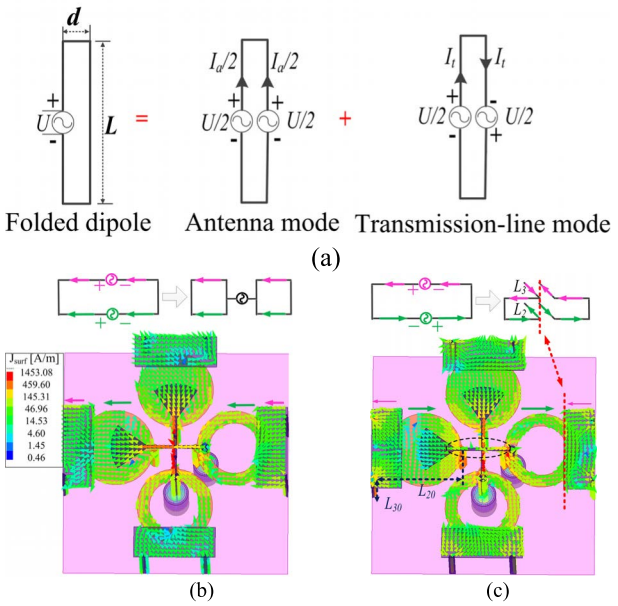

FIGURE 3. Folded dipole and current density vector of reference element I at different frequencies. (a) Folded dipole and its equivalent transmission-line and antenna mode models [26]. (b) Current density vector of reference element I at 9.4 GHz. (c) Current density vector of reference element I at 6.6 GHz.

bandwidth and a poor D-plane scan behavior: (1) there is a spike of the AR at $f_1 = 6.6$ GHz, which is independent of the scanning plane and scanning angle, and seriously affects the scanning AR bandwidth, and (2) with the increase of the scanning angle, the AR in each scanning plane deteriorates. This is especially true during wide-angle scanning in the D-Plane. For example, at $\theta = 45°$, most of the frequency points in the band of interest (4–12 GHz) do not meet the requirement of AR < 3 dB.

B. CAUSES OF THE SCANNING BLIND ZONE

For completeness, we give a brief description of the folded dipole and its equivalent transmission-line and antenna mode models. The interested reader is referred to [26] for a complete presentation on the transmission line model of the folded dipole. A folded dipole can be analyzed by assuming that its current is decomposed into two distinct modes: a transmission-line mode and an antenna mode. The antenna mode divides the folded dipole into separate dipoles. Near $L = \lambda/2$, the transmission-line mode current is small because its input impedance is an open circuit, and the transmission-line mode reduces the antenna to the series connection of two nonradiating $\lambda/4$ stubs. This type of an analytical model is mainly used to predict the input impedance provided the longer parallel wires are close together ($L \gg d$). However, this model helps explain the feasibility of equating Reference Element I, which is in the nonradiating state, with a $\lambda_g/4$ open-circuit two-wire transmission line.

The current density vectors of Reference Element I at different frequency points under the scanning condition (45° scan in xz-plane) are compared, as shown in Figure 3(b) and (c). When $f_2 = 9.4$ GHz, the current distribution on Reference Element I is similar to the antenna mode of the folded dipole, the dipole and the coupling patch are considered as two pairs of parallel dipoles, and the radiation field of the antenna is the superposition of the two pairs of dipoles. As shown in Figure 3(c), at $f_1 = 6.6$ GHz, the current distribution on Reference Element I is similar to the transmission line mode of the folded dipole. Although the tightly coupled environment mitigates the low-frequency AR bandwidth limit, it also causes the transmission line mode to be excited at a certain frequency. The transmission line mode makes two opposite currents appear on the fan-shaped feeding line, resulting in the antenna being unable to work normally, causing the scanning blind zone. In the case where this nonradiating state dominates, Reference Element I is equivalent to two shorted two-wire transmission lines in opposite directions, where the length of the transmission line is $L_1 = \lambda_g/4$, where λ_g is the waveguide wavelength.

In order to shift the transmission line mode out of the frequency band of interest, the shorted two-wire transmission line model is used to quantitatively analyze the relationship between the frequency value corresponding to the axial ratio spike and the structural parameters. A shorted two-wire transmission line can be approximated as an excitation dipole with a length of L_2 and a coupled dipole with a length of L_3, and $L_1 = L_2 + L_3$. The scanning blind zone frequency f_{11} can be calculated according to the shorted two-wire transmission line model:

$$f_{11} = \frac{c}{4\sqrt{\varepsilon_r}(L_2 + L_3)} \tag{1}$$

$$L_2 = \begin{cases} p/2 - l_1 - l_4 + r & l_0 < p/2 - (l_4 + r) \\ p/2 + l_0 - 2l_1 - l_4 + r & l_0 \geq p/2 - (l_4 + r) \end{cases} \tag{2}$$

$$L_3 = \begin{cases} p/2 - l_0 - l_4 - r + h_2 + h_3 + t & l_0 < p/2 - (l_4 + r) \\ l_1 - l_0 + h_2 + h_3 + t & l_0 \geq p/2 - (l_4 + r) \end{cases} \tag{3}$$

where c is the speed of light, using the variables shown in Figure 1. For simplicity of analysis, the transmission line length L_1 is rewritten as: $L_1 = L_{20} + L_{30}$,

$$L_{20} = \begin{cases} p - l_0 - l_1 - 2l_4 & l_0 < p/2 - (l_4 + r) \\ p/2 - l_1 - l_4 + r & l_0 \geq p/2 - (l_4 + r) \end{cases} \tag{4}$$

$$L_{30} = h_2 + h_3 + t \tag{5}$$

Figure 4 and Table 3 show the simulation results (Ansys HFSS) and theoretical calculation values. Considering the parameters that can be adjusted in practice, three parameters h_3, l_0 and ε_r are selected as control variables.

As shown in Figure 4 (b), when $l_0 \geq p/2 - (l_4 + r)$, the calculated frequency is 7.22 GHz, while the simulated value is between 7.3–7.5 GHz. There might be errors in the theoretical model, and there may be other coupling factors that cause the frequency offset. However, overall, the theoretical results are in good agreement with the simulation results, with only a 5.3% frequency error, suggesting the effectiveness for

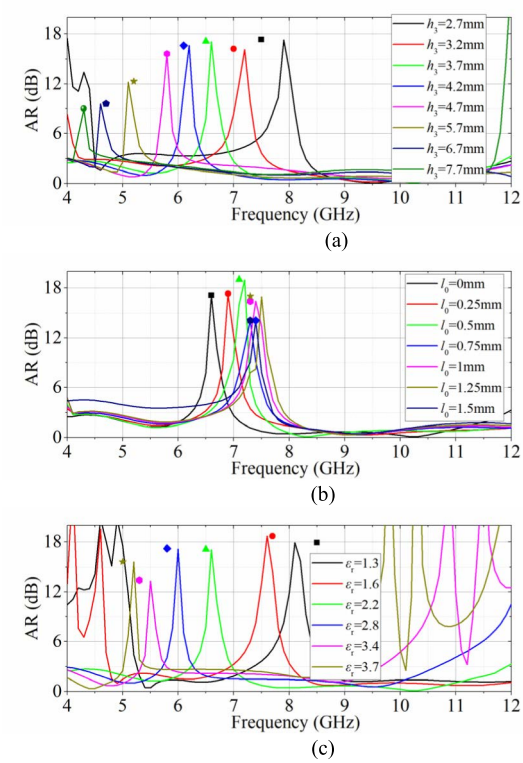

FIGURE 4. Simulation results (solid line) and theoretical calculation values (symbols). (a) h_3. (b) l_0. (c) ε_r.

TABLE 3. Comparison of shorted transmission line model with simulation.

h_3 [mm]	l_0 [mm]	ε_r	Simulation f_1 [GHz]	Theoretical f_1 [GHz]	Error
2.7	0	2.2	7.9	7.48	5.3%
3.2	0	2.2	7.2	6.97	3.2%
3.7	0	2.2	6.6	6.52	1.2%
5.7	0	2.2	5.1	5.18	1.6%
7.7	0	2.2	4.3	4.30	0%
3.7	**0.25**	2.2	6.9	6.74	2.3%
3.7	**0.5**	2.2	7.2	6.97	3.2%
3.7	**0.75**	2.2	7.3	7.22	1.1%
3.7	**1.25**	2.2	7.5	7.22	3.7%
3.7	**1.5**	2.2	7.4	7.22	2.4%
3.7	0	**1.3**	8.1	8.48	4.7%
3.7	0	**1.6**	7.6	7.65	0.5%
3.7	0	**2.8**	6.0	5.78	3.6%
3.7	0	**3.4**	5.5	5.25	4.7%
3.7	0	**3.7**	5.1	5.03	1.3%

the shorted two-wire transmission line model. The following three conclusions are obtained. (1) Instead of shifting the common-mode resonance existing in TCDA antenna out of the high frequency band [12]–[14], an effective solution to deal with this scanning blind zone is to shift it out of the low frequency band, by increasing the length of L_1; (2) An increase in h_1 or ε_r shifts the spike to low frequency. However, after increasing to a certain value, a new spike appears at high frequency; (3) When it does not significantly increase the antenna profile height, L_{20} should be increased. Because the period p should meet the grating lobe condition, the

TABLE 4. Parameters of the Cp-Tcda element.

Parameter	Value (mm)	Parameter	Value (mm)	Parameter	Value (mm)
l_5	0.4	l_6	2	h_4	0.254
l_4	4	r_1	2.4		

adjustment range of the length L_{20} for Reference Element I is limited.

C. SHIFTING THE SCANNING BLIND ZONE OUT-OF-BAND

In order to shift the scanning blind zone out of the low frequency band without increasing the antenna profile, L_{20} needs to be increased as much as possible. In this paper, we increase the length L_{20} through the rotation of dipoles, as shown in Figure 5(a). We can see that L_{21} becomes larger as the rotation angle β increases, which makes it possible to shift the scanning blind zone out of the low frequency band. Figure 5(b) shows the scanning AR at different rotation angles. As the rotation angle β increases, the scanning blind zone gradually shifts to low frequencies. When $\beta = 45°$ (diagonal-direction), the element is referred to as Reference Element II, and the spike of AR is close to the low frequency band edge, which validates the effectiveness of this method.

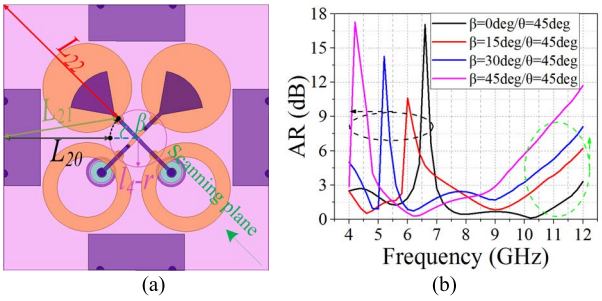

FIGURE 5. Rotation angle scheme. (a) The schematic of element. (b) The AR of the scanning plane ($\theta = 45°$).

III. CP ELEMENT DESIGN AND SIMULATION

In Section II, we proposed and verified the method of rotating the cross dipole to shift the scanning blind zone out of the low frequency band. In this section, based on Reference Element II, the proposed CP-TCDA element is designed, and the performance is assessed via simulation.

A. THE STRUCTURE OF THE PROPOSED CP-TCDA ELEMENT

As shown in Figure 5(a), when $\beta = 45°$, $L_{22} > L_{21} > L_{20}$. If the grounded coupling patch is shifted to the diagonal direction, the length L_1 would further increase, thereby reducing the frequency of the scanning blind zone. In order to ensure the symmetry of the structure, all dipoles are changed to hollow rings, and the sector feeding is changed to a Y-shaped feeding. The proposed CP-TCDA element is shown in Figure 6, the main parameters of which are shown in Table 4. The other parameters are the same as in Table 2.

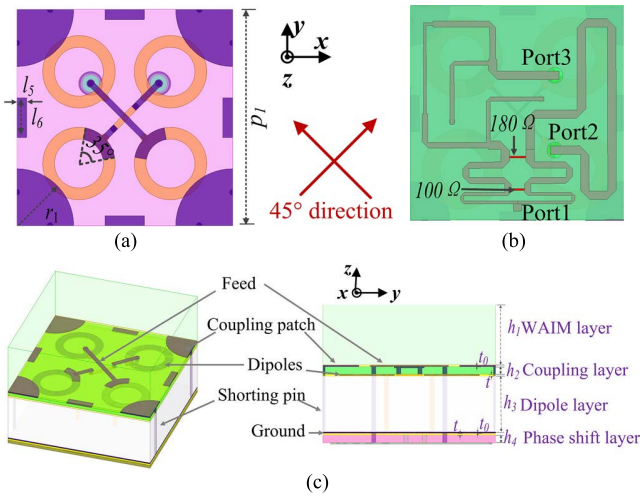

FIGURE 6. The schematic of the proposed CP-TCDA element. (a) Top view. (b) Bottom view (90° phase shifter). (c) Perspective view.

The diagonal-direction (±45° direction) layout topology solves the scanning blind zone problem affecting the scanning AR bandwidth. Next, we study the improvement of the high frequency wide-angle AR on the scanning planes. Due to the symmetry of the proposed CP-TCDA element, the scanning behavior of the *xz*- and D-plane are selected for analysis.

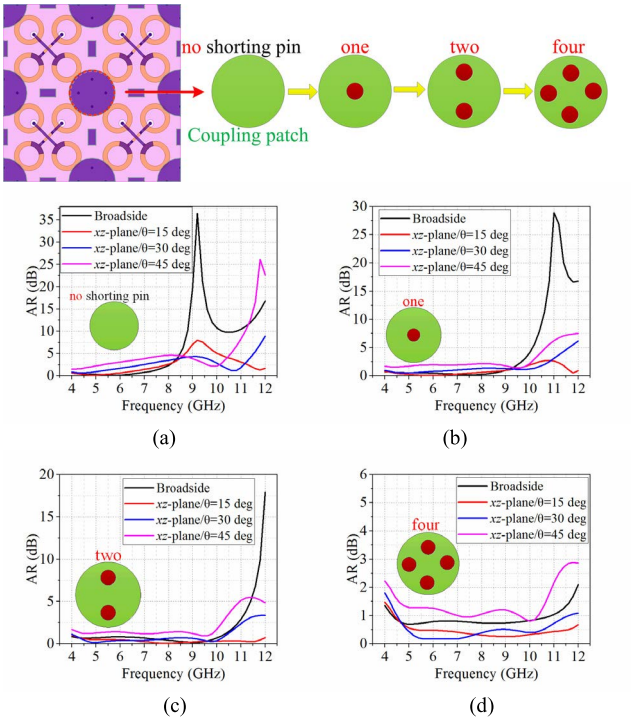

FIGURE 7. The influence of the number of shorting pins on the scanning AR. (a) n = 0. (b) n = 1. (c) n = 2. (d) n = 4.

For *xz*-plane scanning performance, we mainly need to solve the problem of AR deterioration caused by common-mode resonance. Similar to the method of dual-polarization TCDA antenna to expand the impedance bandwidth [13], the common-mode resonance, especially the broadside common-mode resonance, is shifted out of the high frequency band by introducing shorting pins, as shown in Figure 7. The number of shorting pins plays a key role in the scanning AR performance of the *xz*-plane. When the number of shorting pins is $n \leq 2$, the wide-angle AR performance of the high frequency band is poor. As the number of shorting pins increases, the common-mode resonance is gradually shifted out of the high frequency band, and the absolute value of the AR gradually decreases. When $n = 4$, the scanning AR in the *xz*-plane meets the requirement of AR < 3 dB.

In the case of CP beam scanning antennas, the reason for the degradation of AR performance is the difference between horizontal polarization (H-pol) and vertical polarization (V-pol) [27]. As the scanning angle increases, the difference also increases, especially for wide-angle scanning on the D-plane. To improve the D-plane scan behavior, we introduce parasitic strips on the coupling layer. Figure 8 shows the AR curve of the *xz*-plane/D-plane with/without strips, which reveals the influence of parasitic strips on the AR performance in each scanning plane. It shows that after adding the parasitic strips, the scanning AR in the D-plane is improved, within the scanning range of ±60° and the scanning AR on all planes less than 3.5 dB.

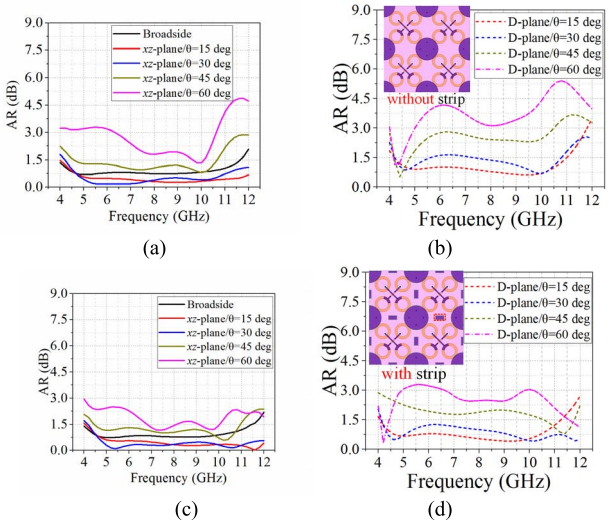

FIGURE 8. The influence of parasitic strips on the scanning AR. (a) Broadside and xz-plane (without strips). (b) D-plane (without strips). (c) Broadside and xz-plane (with strips). (d) D-plane (with strips).

B. THE RESULTS OF THE PROPOSED CP-TCDA ELEMENT

The DP TCDA element arranged along the ±45° direction provides the amplitude conditions, a wideband 90° phase shifter provides a stable phase difference, and then wideband scanning CP element is finally constructed. The measured amplitude and phase characteristic curves of the 90° phase shifter are shown in Figure 9. It is noted that the insertion loss at low frequency band is relatively large (the maximum is 0.8 dB), which may be due to poor matching for the low frequency band. The active VSWR and AR of the proposed CP-TCDA element are shown in Figure 10. There is

a 3:1 (4–12 GHz) overlapping bandwidth within the ±45° angle range for all scanning planes, which meets the requirement of AR < 3 dB. We observed that, except for the D-plane, the proposed CP-TCDA element can reach a broader angle, e.g., a ±60° scan range.

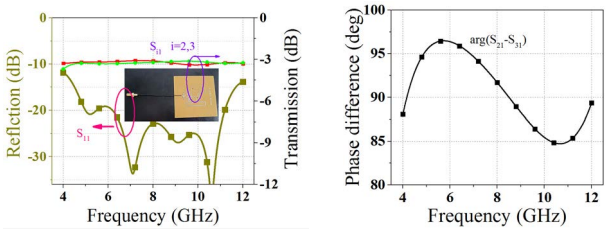

FIGURE 9. The output amplitude and phase characteristics of the 90° phase shifter. (a) Amplitude characteristics. (b) Phase difference.

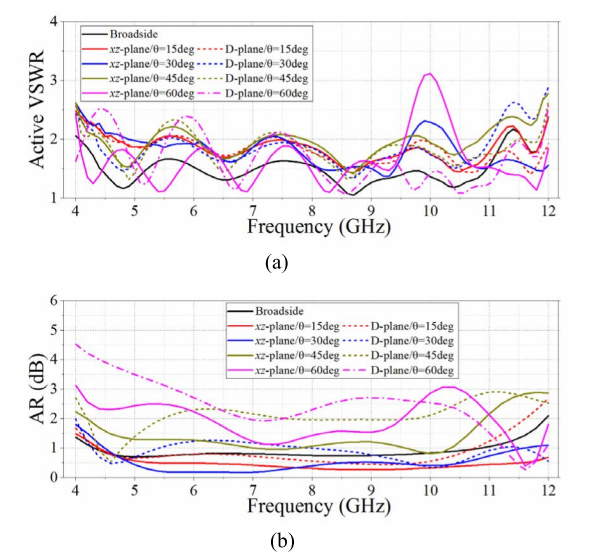

FIGURE 10. The active VSWR and AR of the proposed LHCP-TCDA element. (a) Active VSWR. (b) AR.

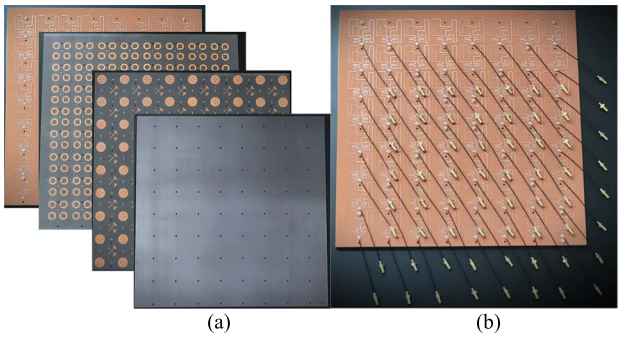

FIGURE 11. The schematic of the wideband scanning CP-TCDA antenna. (a) Top view. (b) Bottom view.

IV. FABRICATION AND MEASUREMENT

An 8 × 8 LHCP planar array antenna based on the proposed CP-TCDA element is designed, fabricated, and tested, as shown in Figure 11. The array antenna is composed of four layers, and technics of the pressing of microwave multilayer printed circuit board lamination is used to ensure effective electrical contact. The outermost elements of the antenna are expanded to maintain the integrity of the circular coupling patches and shorting pins. Figure 12 shows the active VSWRs of the center element and the scanning ARs of the planar array antenna. The measured results show that the proposed CP beam scanning array antenna works well at a 3:1 (4–12 GHz) bandwidth. Within a ±45° scanning angle range, it meets the requirement of AR < 3 dB and active VSWR < 2.9. Some methods can be used to solve the problem that the active VSWR of the proposed array antenna is relatively large. For example, one may use a frequency-selective surface resistive card within the substrate [28] or a printed frequency-selective surface instead of the WAIM layer [29].

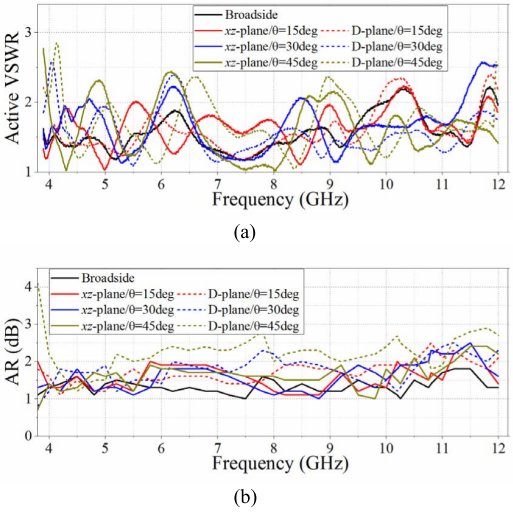

FIGURE 12. The measured active VSWR and AR. (a) Active VSWR of the center element. (b) The ARs of the array antenna.

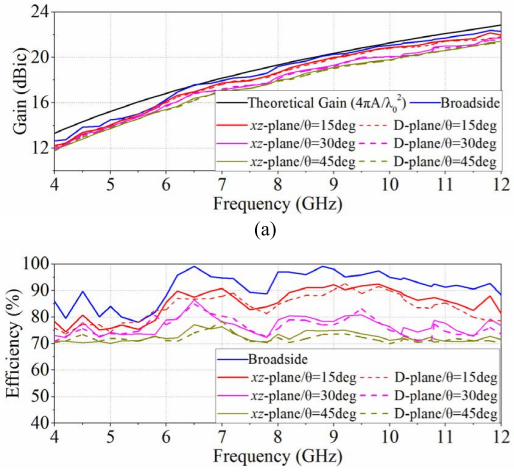

FIGURE 13. The measured realized gains and antenna efficiency at different scanning angles. (a) Measured gains. (b) Antenna efficiency.

Fig. 13 shows the measured realized gain and antenna efficiency in the *xz*-plane and D-plane at different scanning

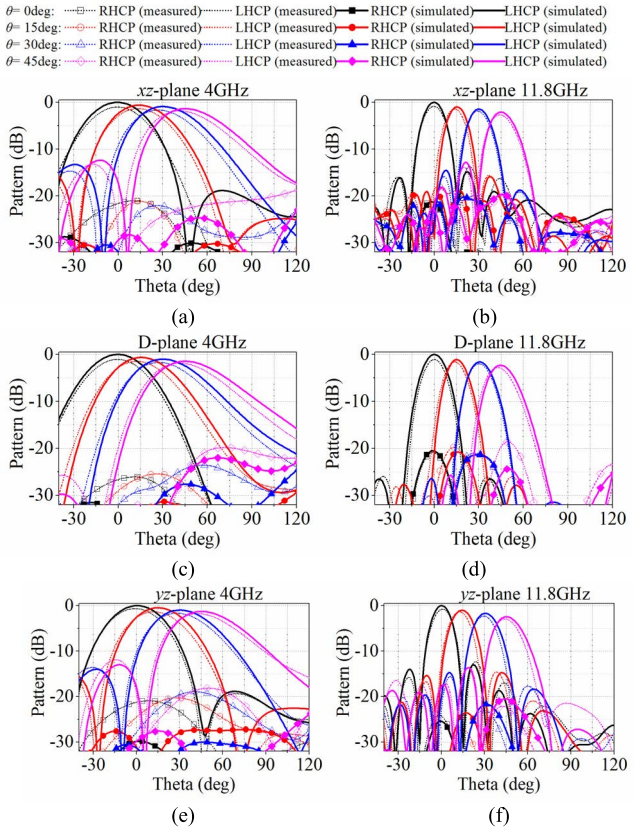

FIGURE 14. Measured (dashed line) and simulated (solid line) scan patterns in the xz-/yz-/D-plane (0°, 15°, 30°, and 45°). The co-polarization (LHCP) components are not labeled, and cross-polarization (RHCP) components are labeled with symbols. (a) *xz*-plane at 4 GHz. (b) *xz*-plane at 11.8 GHz. (c) D-plane at 4 GHz. (d) D-plane at 11.8 GHz. (e) *yz*-plane at 4 GHz. (f) *yz*-plane at 11.8 GHz.

angles. The ideal aperture gain is calculated using $4\pi A/\lambda_0^2$, where A is the aperture area and λ_0 is the wavelength in free space. The efficiency in the entire band exceeds 70% in all scanning planes. Figure 14 shows the radiation patterns for beam scanning in the *xz*-, *yz*-, and D-planes at 4.0, 11.8 GHz, respectively. It can be seen that the measured patterns agree with the simulated ones, and the discrepancies are mainly due to the strong reflection at the edge of the electrically small aperture [30]. The error in the measured beam pointing angle may be caused by the discrete value of the digital phase shifters. The antenna shows a good cross-polarization (RHCP) discrimination (XPD) of better than −15.7 dB at different scanning angles in all scanning planes from 4 to 12 GHz. The side-lobe level is close to is −13 dB at the broadside.

V. CONCLUSION

In this paper, we design a wideband scanning CP TCDA antenna by combining the advantages of CP double-fed structure and TCDA antennas. A simple shorted two-wire transmission line model is proposed, which qualitatively and quantitatively explains the causes of and solutions to the scanning blind zone. The CP-TCDA element arranged along the 45° direction shifts the scanning blind zone out of the low frequency band and ensures the AR performance in all scanning planes. An 8 × 8 LHCP planar array antenna based on the proposed CP-TCDA element is fabricated and tested. The results demonstrate that the antenna achieved a 3:1 (4–12 GHz) overlapping bandwidth within a ±45° scanning angle range.

Future studies will be aimed at introducing the novel feeding and low-profile parasitic structures, which can be used to increase the scanning bandwidth and scanning angle.

REFERENCES

[1] H. Zhang, S. Yang, Y. Chen, J. Guo, and Z. Nie, "Wideband dual-polarized linear array of tightly coupled elements," *IEEE Trans. Antennas Propag.*, vol. 66, no. 1, pp. 476–480, Jan. 2018.

[2] H. Al-Saedi, W. M. Abdel-Wahab, S. M. Raeis-Zadeh, E. H. M. Alian, A. Palizban, A. Ehsandar, N. Ghafarian, G. Chen, S. R. Boroujeni, M.-R. Nezhad-Ahmadi, and S. Safavi-Naeini, "An integrated circularly polarized transmitter active phased-array antenna for emerging Ka-band satellite mobile terminals," *IEEE Trans. Antennas Propag.*, vol. 67, no. 8, pp. 5344–5352, Aug. 2019.

[3] L.-K. Zhang, Y.-X. Wang, J.-Y. Li, Y. Feng, and W. Zhang, "Cavity-backed circularly polarized cross-dipole phased arrays," *IEEE Antennas Wireless Propag. Lett.*, vol. 20, no. 9, pp. 1656–1660, Sep. 2021.

[4] Y.-L. Yao, F.-S. Zhang, and F. Zhang, "A new approach to design circularly polarized beam-steering antenna arrays without phase shift circuits," *IEEE Trans. Antennas Propag.*, vol. 66, no. 5, pp. 2354–2364, May 2018.

[5] R. Movahedinia, A.-R. Sebak, M. R. Chaharmir, M. R. Nikkhah, and A. A. Kishk, "X-band circularly polarized electronically steerable parasitic array radiator of DRA," *IEEE Trans. Antennas Propag.*, vol. 66, no. 2, pp. 721–728, Feb. 2018.

[6] Y. Yang, Y.-L. Ban, Q. Yang, J.-W. Lian, Q. Sun, and G. Wu, "Millimeter wave wide-angle scanning circularly polarized antenna array with a novel polarizer," *IEEE Trans. Antennas Propag.*, vol. 70, no. 2, pp. 1077–1086, Feb. 2022.

[7] Z.-Y. Yu, Y.-H. Zhang, S.-Y. He, H.-T. Gao, H.-T. Chen, and G.-Q. Zhu, "A wide-angle coverage and low scan loss beam steering circularly polarized folded reflectarray antenna for millimeter-wave applications," *IEEE Trans. Antennas Propag.*, vol. 70, no. 4, pp. 2656–2667, Apr. 2022.

[8] P. Liu, Y. Li, and Z. Zhang, "Circularly polarized 2 bit reconfigurable beam-steering antenna array," *IEEE Trans. Antennas Propag.*, vol. 68, no. 3, pp. 2416–2421, Mar. 2020.

[9] R. Hong, J. Shi, D. Guan, W. Cao, and Z. Qian, "Wideband and low-loss beam-scanning circularly polarized antenna based on air-filled SIW," *IEEE Antennas Wireless Propag. Lett.*, vol. 20, no. 7, pp. 1254–1258, Jul. 2021.

[10] J.-W. Kim, S.-C. Chae, H.-W. Jo, T.-D. Yeo, and J.-W. Yu, "Wideband circularly polarized phased array antenna system for wide axial ratio scanning," *IEEE Trans. Antennas Propag.*, vol. 70, no. 2, pp. 1523–1528, Feb. 2022.

[11] B. A. Munk, R. Taylor, T. Durharn, W. Croswell, B. Pigon, R. Boozer, S. Brown, M. Jones, J. Pryor, S. Ortiz, and J. Rawnick, "A low-profile broadband phased array antenna," in *Proc. IEEE Antennas Propag. Soc. Int. Symp.*, Columbus, OH, USA, Jun. 2003, pp. 448–451.

[12] J. P. Doane, K. Sertel, and J. L. Volakis, "A wideband, wide scanning tightly coupled dipole array with integrated balun (TCDA-IB)," *IEEE Trans. Antennas Propag.*, vol. 61, no. 9, pp. 4538–4548, Sep. 2013.

[13] S. S. Holland, D. H. Schaubert, and M. N. Vouvakis, "A 7–21 GHz dual-polarized planar ultrawideband modular antenna (PUMA) array," *IEEE Trans. Antennas Propag.*, vol. 60, no. 10, pp. 4589–4600, Oct. 2012.

[14] J. T. Logan, R. W. Kindt, M. Y. Lee, and M. N. Vouvakis, "A new class of planar ultrawideband modular antenna arrays with improved bandwidth," *IEEE Trans. Antennas Propag.*, vol. 66, no. 2, pp. 692–701, Feb. 2018.

[15] L. Li, J.-B. Yan, C. O'Neill, C. D. Simpson, and S. P. Gogineni, "Coplanar side-fed tightly coupled ultra-wideband array for polar ice sounding," *IEEE Trans. Antennas Propag.*, vol. 70, no. 6, pp. 4331–4341, Jun. 2022.

[16] X. Lv, Y. Zhang, Q. Shi, M. Temiz, and A. El-Makadema, "A dual slant-polarized cylindrical array of tightly coupled dipole antennas," *IEEE Access*, vol. 10, pp. 30858–30869, 2022.

[17] B. Wang, S. Yang, Z. Zhang, Y. Chen, S. Qu, and J. Hu, "A ferrite-loaded ultralow profile ultrawideband tightly coupled dipole array," *IEEE Trans. Antennas Propag.*, vol. 70, no. 3, pp. 1965–1975, Mar. 2022.
[18] L. Zhang, S. Gao, Q. Luo, W. Li, Y. He, and Q. Li, "A wideband circularly polarized tightly coupled array," *IEEE Trans. Antennas Propag.*, vol. 66, no. 11, pp. 6382–6387, Nov. 2018.
[19] T.-L. Zhang, L. Chen, S. M. Moghaddam, A. U. Zaman, and J. Yang, "Millimeter-wave ultrawideband circularly polarized planar array antenna using bold-C spiral elements with concept of tightly coupled array," *IEEE Trans. Antennas Propag.*, vol. 69, no. 4, pp. 2013–2022, Apr. 2021.
[20] P. Zhou, Q. Huang, L. Yang, X. Li, and X. Shi, "Wideband circularly polarised antenna based on interelement mutual coupling effect," *IET Microw., Antennas Propag.*, vol. 14, no. 14, pp. 1803–1807, Nov. 2020.
[21] L. Yang, Z. Zhang, D. Wu, G. Fu, and Z. Yan, "Wideband circularly polarised antenna based on tightly coupling effect," *Electron. Lett.*, vol. 53, no. 7, pp. 448–450, Mar. 2017.
[22] D.-C. Son, A. Samaiyar, M. A. Elmansouri, and D. S. Filipovic, "Design of a circularly-polarized tightly-coupled microstrip patch array," in *Proc. IEEE Int. Symp. Antennas Propag. USNC-URSI Radio Sci. Meeting (APS/URSI)*, Dec. 2021, pp. 513–514.
[23] L. Bian, X.-Q. Shi, and Y.-X. Guo, "Wideband circularly polarised slot antenna," *IET Microw., Antennas Propag.*, vol. 2, no. 5, pp. 497–502, Aug. 2008.
[24] M. H. Novak and J. L. Volakis, "Ultrawideband antennas for multiband satellite communications at UHF-Ku frequencies," *IEEE Trans. Antennas Propag.*, vol. 63, no. 4, pp. 1334–1341, Apr. 2015.
[25] J. Zhong, "Broadband antennas and arrays on conductive textile threads," M.S. dissertation, Ohio State Univ., Columbus, OH, USA, 2017.
[26] G. Thiele, E. Ekelman, and L. Henderson, "On the accuracy of the transmission line model of the folded dipole," *IEEE Trans. Antennas Propag.*, vol. AP-28, no. 5, pp. 700–703, Sep. 1980.
[27] A. Smolders and U. Johannsen, "Axial ratio enhancement for circularly-polarized millimeter-wave phased-arrays using a sequential rotation technique," *IEEE Trans. Antennas Propag.*, vol. 59, no. 9, pp. 3465–3469, Sep. 2011.
[28] A. D. Johnson, J. Zhong, S. B. Venkatakrishnan, E. A. Alwan, and J. L. Volakis, "Phased array with low-angle scanning and 46: 1 bandwidth," *IEEE Trans. Antennas Propag.*, vol. 68, no. 12, pp. 7833–7841, Dec. 2020.
[29] E. Yetisir, N. Ghalichechian, and J. L. Volakis, "Ultrawideband array with 70° scanning using FSS superstrate," *IEEE Trans. Antennas Propag.*, vol. 64, no. 10, pp. 4256–4265, Oct. 2016.
[30] B. A. Munk, "Surface waves on passive surfaces of finite extent," in *Finite Antenna Arrays and FSS*, 1st ed. Hoboken, NJ, USA: Wiley, 2003, pp. 84–135, ch. 4.

MING-YANG ZHAO was born in Yichang, China, in 1987. He received the B.S. degree in electronic information engineering from the Wuhan University of Technology, Wuhan, China, in 2010, and the M.S. degree in electromagnetic fields and microwave technology from the School of Information Engineering University, Zhengzhou, China, in 2013, where he is currently pursuing the Ph.D. degree in information and communication engineering. His research interests include ultra-wideband and wide-angle scanning phased array antennas.

YI-JUN ZHU (Member, IEEE) received the B.Eng., M.Sc., and Ph.D. degrees from the National Digital Switching System Engineering and Technological Research Center (NDSC), Zhengzhou, Henan, China, in 1999, 2002, and 2010, respectively. In 2011, he visited the Department of Electrical and Computer Engineering, McMaster University. He is currently with the School of Information Engineering University. His research interests include the areas of wireless communication theory, visible light communications, and signal processing.

TAO WANG received the B.S. degree in computer communication and the M.S. and Ph.D. degrees in information and communication engineering from the School of Information Engineering University, Zhengzhou, China, in 2000, 2005, and 2011, respectively. His research interests include the areas of wireless communication theory, visible light communications, and signal processing.

TIAN-PENG LI received the B.S., M.S., and Ph.D. degrees from Air Force Engineering University, Xi'an, China, in 2009, 2012, and 2016, respectively. He is currently working at the School of Information Engineering University. His research interests include antenna and propagation.

BEN-LONG XIAO received the B.S. and M.S. degrees from the Equipment Command Technology College, Beijing, China, in 2005 and 2008, respectively. He is currently working at the State Key Laboratory of Complex Electromagnetic Environment Effects on Electronics and Information System. His research interests include electromagnetic environmental effects and protection technology, antenna, and propagation.

FENG-LIANG NIU received the B.S. and M.S. degrees from the National University of Defense Technology, Changsha, China, in 2010 and 2012, respectively. He is currently working at the State Key Laboratory of Complex Electromagnetic Environment Effects on Electronics and Information System. His research interests include electromagnetic environmental effects and protection technology, antenna, and propagation.

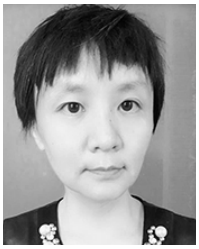

XUE LEI received the B.S. and M.S. degrees from PLA Strategic Support Force Information Engineering University, Zhengzhou, China, in 1989 and 2000, respectively. She is currently working at the School of Information Engineering University. Her research interests include array antenna and smart antenna.